Controllable synthesis of CdSe QDs@NPC composite improving electron–hole separation and enhancing visible-light photocatalytic activities toward RhB degradation

Jiayu Zhu, Ze Wang, Yafeng Li ✉, *Yuanrui Wang*

School of Chemical Engineering, Changchun University of Technology, Changchun 130012, People's Republic of China
✉ *E-mail: liyafeng@ccut.edu.cn*

Published in Micro & Nano Letters; Received on 8th November 2018; Revised on 19th January 2019; Accepted on 27th February 2019

In this work, NPC (nanoporous carbon) is purposely employed to accommodate the semiconductor CdSe QDs (quantum dots) in the absence of any capping agent to facilitate the visible-light photocatalyst CdSe QDs@NPC composite. CdSe QDs@NPC composite has been achieved by the facile method of the incipient-wetness deposition, and furthermore characterised by powder X-ray diffraction, inductively coupled plasma atomic emission spectroscopy, X-ray photoelectron spectroscopy, Brunauer–Emmett–Teller, transmission electron microscopy (TEM) and high-resolution TEM (HRTEM). The results of TEM and HRTEM show that CdSe QDs are implanted into NPC and bound to several nanometres. Both X-ray diffraction and HRTEM indicate that the as-synthesised CdSe QDs belong to the cubic phase. The photocatalytic performance of CdSe QDs@NPC composite has been evaluated by degrading the RhB under visible-light irradiation. NPC as electron acceptor and transport channel can enhance the synergism of CdSe and NPC by improving the electron–hole separation. Furthermore, the photocatalytic mechanism exhibits that h^+ and $O_2^{-\bullet}$ species are the decisive, active species in the degradation process of RhB.

1. Introduction: It is a promising approach that the direct utilisation of sunlight drives the chemical reactions to eliminate the environmental contaminations rising from the social developments and human activities [1–3]. This is really green and environment-friendly route because the utilisation of extra chemical reagent in degradation of contamination would somehow bring out the second-pollution. At this status, the photocatalytic degradation is fairly necessitated to be further explored [4–6]. The precious metals, such as Pt, Pd and so on, are efficiently light-harvesting materials; however, the reserves in the entire biosphere are too rare to meet the demands [7, 8]. Hence, more efforts have been devoted to the cheaper semiconductor materials which can attain the electron–hole separation under the irradiation with ultraviolet light and even visible light [9–11]. In spite of the abundance and cheapness of semiconductor materials, the factors to affect the catalytic performance are quietly complicated, such as crystal phase, particle size, forbidden band, dispersity and stability and so on [12–14]. Among the semiconductor materials, CdSe QD (quantum dot), as an important member of II–VI semiconductor family, has been hugely studied as the visible-light photocatalyst of water-splitting and pollutant treatment because the adsorption band of CdSe QD can extend to 720 nm ($E_g = \sim 1.7$ eV) which almost covers the whole visible-light spectra [15–19]. The distinct feature of CdSe QD is size-dependent electronic and optical properties. However, the small size of CdSe QD prompts the electron–hole recombination and is easily photo-oxidised as well. It is proposed that coupling with the second semiconductor is a way to improve the electron–hole separation and resist the photo-oxidation [20–24].

The carbon materials have extensively been employed to the photocatalytic reactions owing to photo-stability, supporting properties, semiconductor properties, electron acceptor and a transport channel and so on [25]. The properties of carbon materials are intensely affected by sources and treatments. Recently, a new kind of NPC (nanoporous carbon) has been fabricated through MOF materials (metal–organic framework) as the starting materials concerning the virtues of MOF materials, such as three-dimensional network, high crystalline, big specific surface area and uniformed pore [26–28]. Xu *et al.* have illustrated that the NPC made of ZIF-8 not only possesses the high specific surface area but also is implied that the pore size of the NPC is uniformly distributed concerning high crystalline of ZIF-8 [29]. Therefore, besides the inherited merits of carbon materials, the NPC as the supporter would offer the advantages of high dispersity and high content, especially the uniformed particle size of a catalyst which is restricted by the pore size of the NPC. On this account, herein, CdSe QD@NPC composite has purposely been prepared by the facile method of the incipient-wetness deposition in the absence of any capping agent. The photocatalytic performances of CdSe QD@NPC composite are further investigated by the degradation to RhB under visible-light irradiation.

2. Experimental section

2.1. Synthesis of CdSe QDs@NPC composite by the method of incipient-wetness deposition: All reagents in this study were directly used without further purification.

ZIF-8. ZIF-8 was prepared under ambient condition and methanol as the solvent according to [30]. Typically, methanol solutions of $Zn(NO_3)_2{\cdot}6H_2O$ (0.2 M, 1 l) and 2-methylimidazole (0.2 M, 1 l) were mixed under stirring and then allowed to react at room temperature for 24 h without stirring. The product was collected by centrifugation, washed several times with methanol, and vacuum-dried overnight at 60°C. The yield of ZIF-8 was about 21% (depended on 2-methylimidazole).

NPC. The preparation of NPC was carried out according to [31]. 1 g of the as-synthesised ZIF-8 was put into the tubular furnace under N_2 as protection gas and calcined at 800°C for 3 h. Zinc was removed by immersing NPC into 1 M HCl for 6 h. Afterwards, NPC was washed three times with water and dried at 120°C. The yield of NPC was about 23% (depended on ZIF-8).

CdSe QDs@NPC. The adsorption capacities of NPC towards water were firstly investigated. The water was dropwise added to 500 mg of NPC with an injector till the adsorption saturation. The results showed that the most adsorption of NPC to water was about 1 ml/g. $CdCl_2$-H_2O solutions were prepared by dissolving 100 g of $CdCl_2{\cdot}2.5H_2O$ into 100 ml of water. The $CdCl_2$ solution was

transferred into the reaction vessel holding 100 mg NPC by the pipette until the solution was entirely absorbed by NPC. Then, the reaction vessel was purged by the oxygen with N_2 for 0.5 h. The colourless NaHSe/ethanol solution was prepared by reacting 15.8 mg (0.2 mmol) of Se and 15.1 mg (0.4 mmol) of $NaBH_4$ in ethanol solution at 50°C for 0.5 h under N_2 protection. Afterwards, 1 mol/l H_2SO_4 was slowly dropped into the solution to produce H_2Se gas. H_2Se gas was transferred into the reaction vessel with N_2 as a carrier. After the reaction was completed, the product was centrifugally isolated at 5000 rpm and washed three times using ethanol by the method of dispersing and centrifugation, and vacuum-dried overnight at 60°C.

2.2. Characterisation techniques: Powder X-ray diffraction (PXRD) patterns were recorded on a Rigaku D/MAX PC2200 diffractometer for Cu Kα radiation ($\lambda = 1.5406$ Å), with a scan speed of 5°/min. The morphologies and size of the samples were inspected on a transmission electron microscope (TEM) (JEOL-2000ex) and high-resolution TEM (HRTEM) (Tecnai G2 F20S-Twin). X-ray photoelectron spectrometry (XPS) data was acquired using an X-ray photoelectron spectrometer with monochromatic Al Kα X-ray (ESCALABMKLL, VG Co.). N_2 isothermal adsorption experiments were performed at 77 K with TriStar II 3020 (Micromeritics Instrument Corporation) apparatus using nitrogen as the probing gas. The samples were vacuumed for 10 h at 75°C before the data were collected. UV–vis spectra were recorded at UV-1901 spectrometer (Youke, China). The CdSe content was determined by the IRIS Intrepid II ICP instrument (Thermo Electron Corp.). The CdSe QDs @ UIO-66 was dissolved by the H_2SO_4/H_2O_2 and diluted to an appropriate concentration. The elemental analysis found (%, calcd.) for CdSe: 27% (33%).

2.3. Photocatalytic performance of CdSe QDs@NPC: Typically, the photocatalytic catalyst (50 mg) was dispersed in an aqueous solution of RhB (20 ml, 0.02 mmol/l) in a 50 ml round-bottomed flask. The solution pH was adjusted to 2–3 with 1 mol/l HCl. The mixture was firstly stirred with a magnetic stirrer in the dark chamber for 0.5 h to reach complete adsorption equilibrium. After that, the suspension was irradiated by a 500 W halogen lamp. A 420 nm cutoff filter was placed between the reaction system and the light source to eliminate the UV. During the entire process, the solids were kept in suspension by magnetic stirring and air (or oxygen) was continuously bubbled through the reaction mixture at a rate of 20 ml/min to maintain dissolved oxygen content. The photocatalytic activities of the CdSe QDs@NPC were evaluated by monitoring the absorbance of the RhB solution at 554 nm during the degradation. At every 10 min intervals, 1 ml of the aliquots was sampled and centrifuged. The dye concentration of the clear supernatant was then measured with a UV-1901 UV/vis spectrometer.

In the control experiment, the mechanical mixture of equal amount of NPC and CdSe QDs was added to the RhB solution. The blank experiments were also carried out under the same conditions, but no catalyst was added.

3. Results and discussions

3.1. CdSe QDs@NPC characterisation: Seen from the PXRD pattern (Fig. 1*b*), the peak shapes of NPC assigned as the graphite phase also remain the good symmetry for the sake of high crystallinity of ZIF-8 [31]. Furthermore, the diffraction peak positions of the as-synthesised CdSe QDs@NPC conformably match those of cubic phase CdSe ($2\theta = 25.3°$, 42°). The diffraction peaks of CdSe QDs in NPC are broadened and weakened, meaning that the particle size of CdSe QDs is relatively small.

The particle size of CdSe QDs with visible-light activity plays an important role in photocatalysis. Technically, NPC calcined from ZIF-8 with high crystallinity and uniformed pore might effectively restrict the particle size of CdSe QDs and expand the dispersity as well. Experimentally, the incipient-wetness deposition has achieved the purpose in the absence of a capping agent which somehow affects the photocatalysis. The TEM shows that CdSe QDs are implanted in the NPC (Fig. 2*c*). The HRTEM image of CdSe QDs@NPC displays the particle size of CdSe QDs and meanwhile gives rise to lattice fringes of CdSe QDs (Fig. 2*d*). The particle size of CdSe QDs in NPC is observed about several nanometres. The lattice fringe of CdSe QDs is 0.35 nm, which consists of the *d* value of (111) facet ($2\theta = 25.3°$) of cubic phase.

The element types, as well as valence state of the as-synthesised CdSe QDs@NPC, have been inquired by employing X-ray photoelectron spectrometry. The results indicate that the C, N, O, Se and Cd are distributed in CdSe QDs@NPC (Fig. 3). The C1s is assigned to the dissociated carbon (284.6 eV) of NPC. The peak at 398.6 eV is attributed to N1s, coupling with the starting material – ZIF-8($Zn(mIm)_2$). The peak at 531.2 eV belongs to O1s. This indicates that NPC derived from ZIF-8 includes an O element in the form of carboxyl or hydroxyl and N element in the skeleton. The fitting peaks of $Cd3d^5$ (405.3 eV) and $Cd3d^3$ (411.4 eV) display that Cd^{2+} cation exists in CdSe QDs@NPC composition and the fitting peak of Se 3d (54.1 eV) indicates the existence of Se^{2-}.

3.2. Photocatalysis activity: The photocatalytic procedures all include two crucial steps: the adsorption towards the reactants

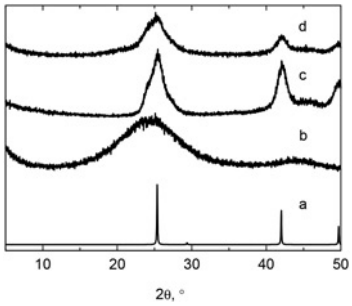

Fig. 1 *PXRD patterns*
a Calculated cubic CdSe from cif.file
b NPC
c CdSe QDs prepared under the same condition in the absence of NPC
d As-synthesised CdSe QDs@NPC

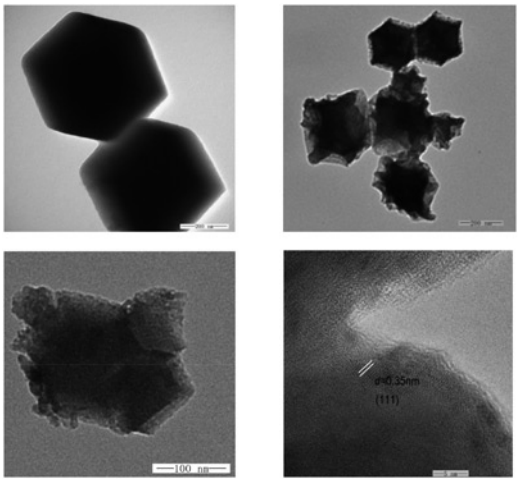

Fig. 2 *TEM and HRTEM diagram*
a TEM diagram of ZIF-8
b TEM diagram of NPC derived from ZIF-8
c TEM diagram of CdSe QDs@NPC
d HRTEM diagram of CdSe QDs@NPC

doi: 10.1049/mnl.2018.5682

and the electron–hole separation triggered by the light irradiation. The higher the adsorption efficiency is, the faster the reaction rate will be on the kinetic theory. As we know, the carbon materials possess powerful adsorption to organic species. Identically, NPC derived from the ZIF-8 shows the strong adsorption ability. Besides, the NPC as the electron acceptor can afford the electron transfer channel, which prompts the electron–hole separation. The light adsorption range of CdSe QDs extends up to 720 nm, which almost covers the visible-light zone. In this context, the photocatalytic abilities of CdSe QDs@NPC are investigated by the degradation of RhB under visible-light irradiation.

In the beginning, the adsorption of CdSe QDs@NPC to reactant RhB is attained to the saturation under the dark chamber. The results show that the concentration of RhB declines by about 30% with the addition of pure NPC in 0.5 h. The concentration of RhB declines by about 18% with the addition of CdSe QDS@NPC in 0.5 h. Thus, the photocatalytic experimental in this context will be proceeded after be adsorbed for 0.5 h under a dark chamber.

As shown in Fig. 4, after adsorbed in a dark chamber for 0.5 h, RhB has basically been degraded in 60 min under the visible-light irradiation with the presence of CdSe QDs@NPC. The photocatalysis obeys the pseudo-first-order kinetic model. To verify the synergism of CdSe and NPC, a mechanical mixture of equal amount of CdSe and NPC is used to the photocatalytic degradation of RhB. The degradation efficiency of the mechanical mixture of CdSe QDs and NPC to RhB is low below 40%. Also, a blank experiment at the absence of any catalyst is done under the same conditions. The photocatalytic results show that the photodegradation of RhB rarely occurs.

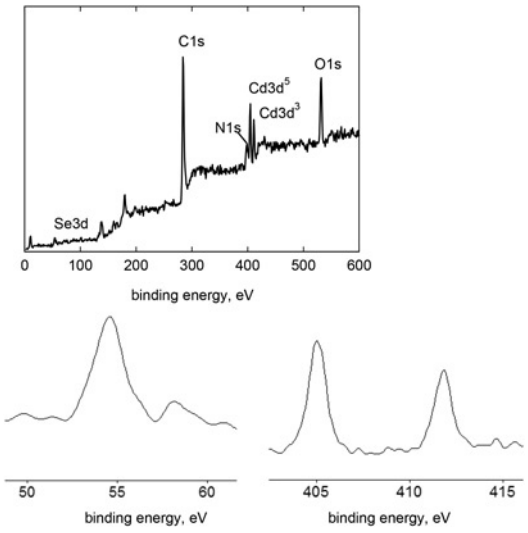

Fig. 3 *XPS survey and fitting peak*
A XPS survey of CdSe QDs@NPC
B Fitting peak of Se^{2-}
C Fitting peak of Cd^{2+}

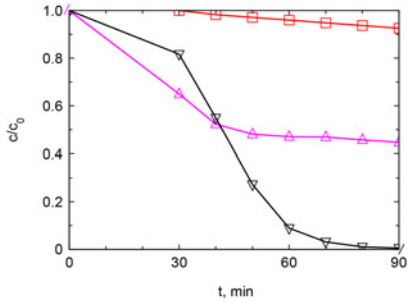

Fig. 4 *Photocatalytic degradation of RhB under visible-light. Down-pointing triangle indicates the CdSe QDs@NPC; up-pointing triangle indicates the control mixture of CdSe QDs and NPC; white square indicates the blank experiment*

3.3. Photocatalytic stability: The photocatalytic stability of CdSe QDs@NPC is assessed with a comparison to PXRD of reacted CdSe QDs@NPC. As illustrated in Fig. 5, the intensity and position of peaks between the as-synthesised CdSe QDs@NPC and used CdSe QDs@NPC are identical, indicating the stability of CdSe QDs@NPC. The stability of CdSe QDs@NPC is further studied by recycling the reacted CdSe QDs@NPC (Fig. 6). After every cycle, the degradation rate of RhB declines by approximately about 3%, which probably arises from the loss of CdSe QDs@NPC.

3.4. Photocatalytic mechanism: The hydroxyl radicals ($HO^{\bullet}$), superoxide radicals ($O_2^{-\bullet}$), and holes (h^+) are three crucial active species referred to the photocatalytic oxidation process. To experimentally testify the photocatalytic mechanism of CdSe QDs@NPC to RhB degradation, isopropyl alcohol (IPA), benzoquinone (BQ), and ethylenediaminetetraacetic acid (EDTA) are introduced into the reaction system to entrap $HO^{\bullet}$, $O_2^{-\bullet}$ and h^+, respectively. The effects of these scavengers as well as of N_2 purging on the photocatalytic activity of CdSe QDs@NPC are shown in Fig. 7.

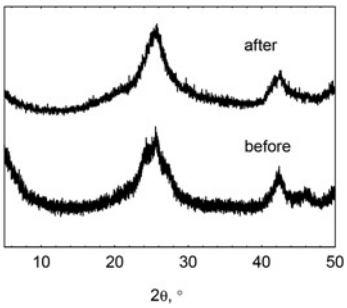

Fig. 5 *PXRD patterns of CdSe QDs@NPC before and after the reaction*

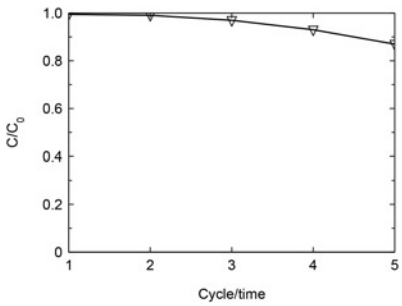

Fig. 6 *Reuses of CdSe QDs@NPC catalyst*

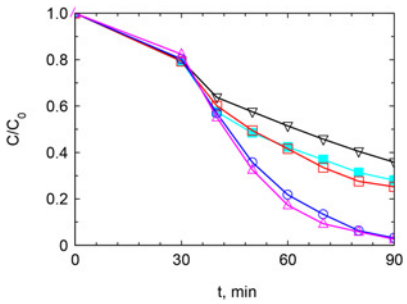

Fig. 7 *Effect of different scavenger and N_2 purging on the degradation of RhB by CdSe QDs@NPC under visible-light irradiation. Up-pointing triangle indicates CdSe QDs@NPC; open circle indicates IPA (0.5 mM); white square indicates EDTA (1 mM); black square indicates QB 1 mM); down-pointing triangle indicates N_2 purging*

The introduction of IPA virtually has no influences on the RhB degradation rate, meaning that $HO^{\bullet}$ is not the main active species. However, the degradation rate decreases significantly since the introduction of BQ, which can quench $O_2^{-\bullet}$. Thus, $O_2^{-\bullet}$ is identified as the major active species for the decomposition of RhB. Since dissolved O_2 is required for the generation of $O_2^{-\bullet}$, the role of $O_2^{-\bullet}$ in the degradation process is validated by purging the dye solution with N_2 to decrease the amount of dissolved O_2. The result demonstrates the negative effect of N_2 purging on the degradation rate. Hence, this result further indicates that $O_2^{-\bullet}$ is an important species. EDTA was added to the system to suppress h^+. The introduction of EDTA significantly lowers the degradation rate, thereby implying that RhB can also be oxidised by the photogenerated h^+ in CdSe QDs@NPC. Therefore, $O_2^{-\bullet}$ and h^+ are the main active species in the degradation process of RhB by the CdSe QDs@NPC photocatalyst.

4. Conclusion: In a sum, through the method of the incipient-wetness deposition, CdSe QDs have purposely been implanted into NPC derived from ZIF-8 in the absence of any capping agent. Also, NPC as the electron acceptor and electron transport channel can improve the electron–hole separation. The synergism of CdSe and NPC enhances the photocatalytic performance. The mechanism experiment indicates that the photogenerated h^+ and $O_2^{-\bullet}$ species are responsible for the photocatalytic activity.

5 References

[1] Hoffmann M.R., Martin S.T., Choi W., *et al.*: 'Environmental applications of semiconductor photocatalysis', *Chem. Rev.*, 1995, **95**, pp. 69–96, doi: 10.1021/cr00033a004

[2] Linic S., Christopher P., Ingram D.B.: 'Plasmonic-metal nanostructures for efficient conversion of solar to chemical energy', *Nat. Mater.*, 2011, **10**, pp. 911–921, doi: 10.1038/nmat3151

[3] Paola A.D., García-López E., Marci G., *et al.*: 'A survey of photocatalytic materials for environmental remediation', *J. Hazard. Mater.*, 2012, **211-212**, pp. 3–29, doi: 10.1016/j.jhazmat.2011.11.050

[4] Chen C., Ma W., Zhao J., *et al.*: 'Semiconductor-mediated photodegradation of pollutants under visible-light irradiation', *Chem. Soc. Rev.*, 2010, **39**, pp. 4206–4219, doi: 10.1039/B921692H

[5] Li H.J., Zhou Y., Tu W.G., *et al.*: 'State-of-the art progress in diverse heterostructured photocatalysts toward promoting photocatalytic performance', *Adv. Funct. Mater.*, 2015, **25**, pp. 998–1013, doi: 10.1002/adfm.201401636

[6] Sun M.H., Huang Z., Chen L.H., *et al.*: 'Applications of hierarchically structured porous materials from energy storage and conversion, catalysis, photocatalysis, adsorption, separation, and sensing to biomedicine', *Chem. Soc. Rev.*, 2016, **45**, pp. 3479–3563, doi: 10.1039/C6CS00135A

[7] Fang X.Z., Shang Q.C., Wang Y., *et al.*: 'Single Pt atoms confined into a metal–organic framework for efficient photocatalysis', *Adv. Mater.*, 2018, **30**, pp. 1705112–1705118, doi: 10.1002/adma.201705112

[8] Li B.X., Wang R.S., Shao X.K., *et al.*: 'Synergistically enhanced photocatalysis from plasmonics and a co-catalyst in Au@ZnO–Pd ternary core–shell nanostructures', *Inorg. Chem. Front.*, 2017, **4**, pp. 2088–2096, doi: 10.1039/C7QI00586E

[9] Lee S.K., Mills A., O'Rourke C.: 'Action spectra in semiconductor photocatalysis', *Chem. Soc. Rev.*, 2017, **46**, pp. 4877–4894, doi: 10.1039/C7CS00136C

[10] Kisch H.: 'Semiconductor photocatalysis for chemoselective radical coupling reactions', *Acc. Chem. Res.*, 2017, **50**, pp. 1002–1010, doi: 10.1021/acs.accounts.7b00023

[11] Zhong D.L., Liu W.W., Tan P.F., *et al.*: 'Insights into the synergy effect of anisotropic {001} and {230} facets of $BaTiO_3$ nanocubes sensitized with CdSe quantum dots for photocatalytic water reduction', *Appl. Catal. B, Environ.*, 2018, **227**, pp. 1–12, doi: 10.1016/j.apcatab.2018.01.009

[12] Spasiano D., Marotta R., Malato S., *et al.*: 'Solar photocatalysis: materials, reactors, some commercial, and pre-industrialized applications. a comprehensive approach', *Appl. Catal. B, Environ.*, 2015, **170-171**, pp. 90–123, doi: 10.1016/j.apcatab.2014.12.050

[13] Zheng D.D., Zhang G.G., Wang X.C.: 'Integrating CdS quantum dots on hollow graphitic carbon nitride nanospheres for hydrogen evolution photocatalysis', *Appl. Catal. B, Environ.*, 2015, **179**, pp. 479–488, doi: 10.1016/j.apcatab.2015.05.060

[14] Wang M.Y., Ioccozia J., Sun L.: 'Inorganic-modified semiconductor TiO_2 nanotube arrays for photocatalysis', *Energy Environ. Sci.*, 2014, **7**, pp. 2182–2202, doi: 10.1039/C4EE00147H

[15] Zhao J., Holmes M.A., Osterlo F.E.: 'Quantum confinement controls photocatalysis: a free energy analysis for photocatalytic proton reduction at CdSe nanocrystal's', *ACS Nano*, 2013, **7**, pp. 4316–4325, doi: 10.1021/nn400826h

[16] Peng X.G., Manna L., Yang W.D.: 'Shape control of CdSe nanocrystals', *Nature*, 2000, **404**, pp. 59–61, doi: 10.1038/35003535

[17] Aguilera-Sigala J., Bradshaw D.: 'Synthesis and applications of metal-organic framework–quantum dot (QD@MOF) composites', *Coord. Chem. Rev.*, 2016, **307**, pp. 267–291, doi: 10.1016/j.ccr.2015.08.004

[18] Chuang C.H., Doane T.L., Lo S.S.: 'Measuring electron and hole transfer in core/shell nanoheterostructures', *ACS Nano*, 2011, **5**, pp. 6016–6024, doi: 10.1021/nn201788f

[19] Qiu F., Han Z.J., Peterson J.J.: 'Photocatalytic hydrogen generation by CdSe/CdS nanoparticles', *Nano Lett.*, 2016, **9**, pp. 5347–5352, doi: 10.1021/acs.nanolett.6b01087

[20] Pan J.H., Dou H.Q., Xing Z.G.: 'Porous photocatalysts for advanced water purification', *J. Mater. Chem.*, 2010, **20**, pp. 4512–4528, doi: 10.1039/B925523K

[21] Tvrdy K., Kamat P.V.: 'Photoinduced electron transfer from semiconductor quantum dots to metal oxide nanoparticles', *Proc. Natl. Acad. Sci.*, 2011, **108**, pp. 29–34, doi: 10.1073/pnas.1011972107

[22] Gerischer H., Luebke M.: 'A particle size effect in the sensitization of TiO_2 electrodes by a CdS deposit', *J. Electroanal. Chem.*, 1986, **204**, pp. 225–227, doi: 10.1016/0022-0728(86)80520-4

[23] Hotchandani S., Kamat P.V.: 'Charge-transfer processes in coupled semiconductor systems: photochemistry and photoelectrochemistry of the colloidal CdS-ZnO system', *J. Phys. Chem.*, 1992, **96**, pp. 6834–6839, doi: 10.1021/j100195a056

[24] Nasr C., Hotchandani S., Kamat P.V.: 'Cdse/SnO_2 coupled semiconductor films. Electrochemical and photoelectrochemical studies', *Proc. Ind. Acad. Sci.*, 1995, **107**, pp. 699–708, doi: 10.1047/j200273b003

[25] Cao S.W., Yu J.G.: 'Carbon-based H_2-production photocatalytic materials', *J. Photochem. Photobiol. C, Photoch. Rev.*, 2016, **27**, pp. 72–99, doi: 10.1016/j.iphotochemrev.2016.04.002

[26] Liu B., Shioyama H., Akita T.: 'Metal-organic framework as a template for porous carbon synthesis', *J. Am. Chem. Soc.*, 2008, **130**, pp. 5390–5391, doi: 10.1021/ja7106146

[27] Tang J., Liu J., Torad N.L.: 'Tailored design of functional nanoporous carbon materials toward fuel cell applications', *Nano Today*, 2014, **9**, pp. 305–323, doi: 10.1016/j.nantod.2014.05.003

[28] Chen Y.Z., Zhang R., Jiao L.: 'Metal–organic framework-derived porous materials for catalysis', *Coord. Chem. Rev.*, 2018, **362**, pp. 1–23, doi: 10.1016/j.ccr.2018.02.008

[29] Jiang H.L., Liu B., Lan Y.Q.: 'From metal-organic framework to nanoporous carbon: toward a very high surface area and hydrogen uptake', *J. Am. Chem. Soc.*, 2011, **133**, pp. 11854–11857, doi: 10.1021/ja203184k

[30] Lu G., Li S.Z., Guo Z.: 'Imparting functionality to a metal–organic framework material by controlled nanoparticle encapsulation', *Nat. Chem.*, 2012, **4**, pp. 310–316, doi: 10.1038/nchem.1272

[31] Torad N.L., Hu M., Kamachi Y.: 'Facile synthesis of nanoporous carbons with controlled particle sizes by direct carbonization of monodispersed ZIF-8 crystals', *Chem. Commun.*, 2013, **49**, pp. 2521–2523, doi: 10.1039/C3CC38955C

doi: 10.1049/mnl.2018.5682